UDE-based Robust Control of a Quadrotor-Slung-Load System*

Yanhu Wang[1,2], Gan Yu[2], Wei Xie[1], Weidong Zhang[3,1], and Carlos Silvestre[2,4]

***Abstract*— This article addresses the robust trajectory tracking problem for a Quadrotor-Slung-Load System (QSLS), which consists of a point-mass load and a rigid-body quadrotor connected by an inelastic cable. To construct the controller, we employ the backstepping technique and propose an Uncertainty and Disturbance Estimator (UDE) to compensate for uncertainties arising from imprecise model parameters and exogenous time-varying disturbances affecting both quadrotor and load. The main feature of the UDE is its ability to convert the robust control problem into a low-pass filter design in the frequency domain, which generates an estimate of lumped uncertainties. To streamline the design process, we utilize a coordinate transformation strategy that converts the QSLS into a configuration that resembles the dynamics of a typical quadrotor system. The proposed controller ensures uniformly ultimate boundedness of closed-loop errors in the presence of time-varying exogenous disturbances, while guaranteeing asymptotic stability when disturbances are zero. Finally, we present comprehensive simulation and experimental results to validate the effectiveness and robustness of the proposed solution.**

I. Introduction

A. Motivation

A diverse array of aerial cable-suspended load transportation tasks finds widespread utilization in industrial operations. These tasks encompass critical functions such as emergency response, search and rescue missions in hazardous scenarios, and heavy equipment delivery [1]–[3].

*Manuscript received: May, 9, 2023; Revised July, 1, 2023; Accepted August, 24, 2023.

This paper was recommended for publication by Editor Clement Gosselin upon evaluation of the Associate Editor and Reviewers' comments.

This work was supported in part by the National Key R&D Program of China under Grant 2022ZD0119901, in part by the Shanghai Science and Technology program under Grant 22015810300 and Grant 19510745200, in part by the Hainan Province Science and Technology Special Fund under Grant ZDYF2021GXJS041, in part by the National Natural Science Foundation of China under Grant U2141234 and Grant 62203297, in part by the Oceanic Interdisciplinary Program of Shanghai Jiao Tong University under Grant SL2022PT112, in part by Macau Science and Technology Development Fund under Grant FDCT/0031/2020/AFJ, in part by the University of Macau, Macau, China, under Grants MYRG2020-00188-FST and MYRG2022-00205-FST, and in part by the Fundação para a Ciência e a Tecnologia (FCT) through ISR LARSyS-FCT Project under Grant UIDB/50009/2020. (*Corresponding author: Wei Xie and Weidong Zhang.*)

[1]Yanhu Wang, Wei Xie, and Weidong Zhang are with the Department of Automation, Shanghai Jiao Tong University, Shanghai 200240, China {wangyanhu, weixie}@sjtu.edu.cn

[2]Yanhu Wang, Gan Yu, and Carlos Silvestre are with the Department of Electrical and Computer Engineering, Faculty of Science and Technology, University of Macau, Macau, China {ganyu, csilvestre}@um.edu.mo

[3]Weidong Zhang is with the School of Information and Communication Engineering, Hainan University, Haikou 570228, Hainan, China {wdzhang}@sjtu.edu.cn

[4]Carlos Silvestre is on leave from the Instituto Superior Técnico, Universidade de Lisboa, 1049-001 Lisbon, Portugal

Digital Object Identifier (DOI): see top of this page.

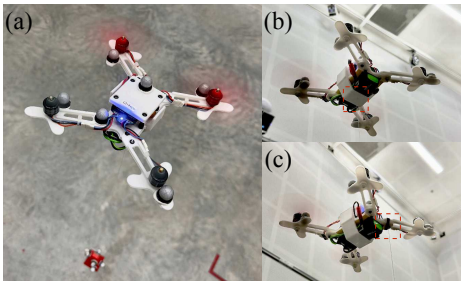

Fig. 1. (a) Main perspective of the QSLS; (b) the load is tethered close to the center of mass of the quadrotor; (c) the load is deliberately tethered away from the center of mass of the quadrotor.

Nevertheless, the successful execution of these missions hinges significantly on the capabilities of human pilots to adeptly handle the load's swing motion, a process fraught with inherent risks and substantial costs. Driven by a vision of cost reduction and a commitment to enhancing operational precision and safety, the research community has dedicated extensive efforts to explore innovative solutions. Their focus revolves around attaining robotic autonomy in aerial load transportation, employing the capabilities of quadrotor vehicles to accomplish this ambitious goal [4]–[8]. See Fig. 1 for an example of a Quadrotor-Slung-Load System (QSLS).

Nevertheless, aerial load transportation using quadrotors remains a challenging problem, with the system's vulnerability to unknown dynamics caused by uncertain system parameters and exogenous disturbances. These include wind disturbances [9], unknown payload mass and cable length [10], and offsets of the tethered point [11] (refer to case (c) in Fig. 1), among many others. The presence of unknown dynamics can significantly compromise system performance, making it crucial to develop robust controllers for successful aerial load transportation automation. In this paper, we will resort to Uncertainty and Disturbance Estimator (UDE) to accurately estimate these adverse impacts, subsequently enabling effective compensation measures.

B. Proposed Solution

The aim of this study is to develop a robust controller employing UDEs for the QSLS, which can ensure that the load follows a predefined trajectory, even when confronted with unknown time-varying uncertainties and disturbances.

The highlights and contributions of our strategy are as follows: (i) the proposed controller accounts for the complete system dynamics, encompassing the underactuation of the quadrotor, the dynamic couplings between the quadrotor and the load, and the swing motion of the load; (ii) all of the uncertain model dynamics, external disturbances acting on both the quadrotor and the load, as well as partial nonlinear

dynamics associated with the vehicle underactuation are lumped into two vector terms, and are ultimately estimated by two UDEs; (iii) the proposed UDEs possess the unique feature of solely utilizing the system inputs and states information, without necessitating time derivatives of states (as opposed to conventional integral backstepping [12] and adaptive neural networks [13]), thereby reducing computational requirements and controller complexity; (iv) sufficient conditions are provided to ensure the cable remains under tension (as opposed to the control methods e.g. in [14]–[16] which rely merely on assumptions); (v) in the presence of disturbances, the proposed controller ensures that the error system's origin is rendered Uniformly Ultimately Bounded (UUB), additionally, it achieves asymptotic stability when disturbances are absent (i.e., zero); and (vi) comprehensive simulation and experimental results (including comparisons with the state-of-the-art results) obtained from a physical QSLS validate the effectiveness and practicality of our proposed strategy.

C. Related Works

Autonomous slung-load transportation using quadrotors was pioneered in [17], [18], and these iconic works arguably established two paradigms: guaranteeing a swing-free transportation for the entire maneuver [17], and allowing for large-swing angles while still ensuring accurate trajectory tracking [18]. Later, diversified approaches to realize the automation of slung-load transportation sprang up, including control [19], motion planning [20] and the use of sensors for state estimate [21], to name just a few.

The QSLS is inevitably affected by unknown dynamics, leading to a substantial impact on the closed-loop system performance. To achieve controller robustness against unknown dynamics, various techniques have been employed, including integral backstepping [12], adaptive neural network [13], nonlinear model predictive controller augmented with an $\mathcal{L}_1$ adaptive controller [22], disturbance observer [23], [24], and UDE [25], among others. Recent advanced control approaches addressing dynamic uncertainties for QSLS are summarized as follows. By leveraging the benefits of artificial neural networks, an adaptive strictly negative imaginary controller was designed in [11] for trajectory tracking under parameter uncertainties. In [26], a nonlinear model predictive control was designed for a quadrotor with a slung-load to stabilize the movements of the load and the quadrotor. However, the controllers in [11], [26] require real-time solution of an optimal control problem, which can be computationally expensive, particularly for the fast dynamics of quadrotors. To overcome the aforementioned limitation, the authors of [16] devised a robust controller using integral backstepping. However, this approach still falls short as the integral actions demand high-order time derivatives of the system states. The controllers in [27], [28] used disturbance observers to compensate for the effects caused by the load swing, wind gusts, and partial rotor failure, but disturbance observers involve taking the inverse of the nominal model in the frequency domain leading to the limited applicability. The authors of [29] developed a UDE-based controller to tackle the path-following problem, compensating for both constant and low-frequency components of disturbances using a low-pass filter. While the controller in [29] uses numerical differentiation, causing severe signal delays and compromising experimental performance.

II. Notation

Throughout the paper, a bold symbol stands for a multi-dimensional variable, e.g., $\mathbf{p}$. Desired values are represented with a subscript $(\cdot)_d$, e.g., $\mathbf{p}_d$. Quantities relating to the quadrotor and load are denoted with subscripts $(\cdot)_Q$ and $(\cdot)_L$, respectively. Also, subscripts $(\cdot)_{\mathbf{y}}$, $(\cdot)_{\mathbf{x}}$, and $(\cdot)_{\bar{\mathbf{x}}}$ are employed to denote the state vectors for the $\mathbf{y}$ system, the $\mathbf{x}$ system, and the $\mathbf{x}$ system when all tracking errors are zero, respectively. Let s represent the Laplace operator, $\mathcal{L}(\bullet)$ denote the Laplace transformation and $\mathcal{L}^{-1}(\bullet)$ is its inverse. The symbols $\mathbf{I}$ and $\mathbf{0}$ denote respectively an identity matrix and a zero matrix of appropriate dimension, and $\otimes$ denotes the Kronecker product. For $\mathbf{a},\ \mathbf{b} \in \mathbb{R}^3$, the map $\mathbf{S}(\mathbf{a}) : \mathbb{R}^3 \mapsto \mathbb{R}^{3\times 3}$ is the skew-symmetric matrix satisfying $\mathbf{S}(\mathbf{a})\mathbf{b} := \mathbf{a} \times \mathbf{b}$ and $\mathbf{S}(\mathbf{a})\mathbf{a} = \mathbf{0}$, and the map $\mathbf{\Pi} : \mathbf{S}^2 \mapsto \mathbb{R}^{3\times 3}$ is defined as $\mathbf{\Pi}(\mathbf{a}) := -\mathbf{S}(\mathbf{a})^2 = \mathbf{I} - \mathbf{a}\mathbf{a}^\mathsf{T}$ satisfying $\mathbf{S}(\mathbf{a})\mathbf{\Pi}(\mathbf{a}) = \mathbf{S}(\mathbf{a})$. Let $\|\mathbf{a}\| := \sqrt{\mathbf{a}^\mathsf{T}\mathbf{a}}$ represent the Euclidean norm of vector $\mathbf{a} \in \mathbb{R}^n$, whose supremum and infimum are respectively given by $\sup_{t\geq 0}\|\mathbf{a}\|$ and $\inf_{t\geq 0}\|\mathbf{a}\|$. Given two sets $\Omega_1 \in \mathbb{R}^n$ and $\Omega_2 \in \mathbb{R}^m$, a function $f : \Omega_1 \mapsto \Omega_2$ is denoted as $f \in (\Omega_1,\ \Omega_2)$, and particularly, in the case of $\Omega_1 = \mathbb{R}_{\geq 0}$, $f \in \Omega_2$ is adopted for brevity. Finally, let $f \in \mathcal{C}^n(\Omega)$ represent $f \in \Omega$ and f is of class at least $\mathcal{C}^n$.

III. System Model with Two States

In the QSLS, the quadrotor is considered as a rigid body with six degrees of freedom, and the point-mass load with two degrees of freedom is attached to the center of mass of the vehicle by a massless cable. We assume for now the cable is always taut and later in Section V, we provide conditions for this to be always valid. We consider a body frame $\{B\}$ that coincides with the center of mass of a quadrotor and a fixed inertial frame $\{I\}$, as shown in Fig. 2. Throughout the rest of the article, all vectors are expressed in the inertial coordinate frame $\{I\}$ unless otherwise stated. The coordinate transformation matrix which maps the vectors in $\{B\}$ into the vectors in $\{I\}$ is denoted as $\mathbf{R} \in SO(3)$, and the quadrotors attitude kinematics is $\dot{\mathbf{R}} = \mathbf{R}\mathbf{S}(\boldsymbol{\omega}_Q)$, where $\boldsymbol{\omega}_Q$ is the angular velocity expressed in $\{B\}$.

Let us consider the following state of the QSLS,

$$\mathbf{y} := [\mathbf{p}_Q^\mathsf{T},\ \mathbf{p}_L^\mathsf{T},\ \mathbf{v}_Q^\mathsf{T},\ \mathbf{v}_L^\mathsf{T}]^\mathsf{T} \in \Omega_{\mathbf{y}} \tag{1}$$

which provide a comprehensive description of the load position and cable attitude subsystems, where the domain $\Omega_{\mathbf{y}} := \{\mathbf{y} \in \mathbb{R}^{12} : \|\mathbf{p}_Q - \mathbf{p}_L\| = \ell,\ (\mathbf{p}_Q - \mathbf{p}_L)^\mathsf{T}(\mathbf{v}_Q - \mathbf{v}_L) = 0\}$; ℓ is the length of the cable; and $\mathbf{p}_{L/Q}$ and $\mathbf{v}_{L/Q}$ represent the position and linear velocity of the load/quadrotor, respectively. To the $\mathbf{y}$ system, the control input is $\mathbf{u}_{\mathbf{y}} := [T,\ \mathbf{r}^\mathsf{T}]^\mathsf{T}$, where $T \in \mathbb{R}_{\geq 0}$ is the quadrotor thrust and $\mathbf{r} := \mathbf{R}\mathbf{e}_3$. Based

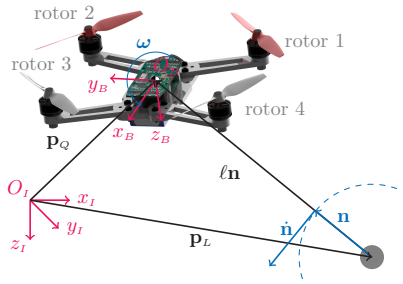

Fig. 2. A sketch of the QSLS.

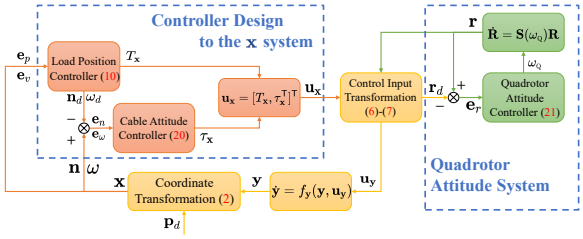

Fig. 3. Flowchart of the proposed controller for the QSLS.

on the state $\mathbf{y}$ defined in (1), we introduce a new state $\mathbf{x} \in \Omega_{\mathbf{x}}$ as

$$\mathbf{x}(\mathbf{y},\ \mathbf{p}_d) := \begin{bmatrix} \mathbf{e}_p \\ \mathbf{e}_v \\ \mathbf{n} \\ \boldsymbol{\omega} \end{bmatrix} := \begin{bmatrix} \mathbf{p}_L - \mathbf{p}_d \\ \mathbf{v}_L - \dot{\mathbf{p}}_d \\ (\mathbf{p}_Q - \mathbf{p}_L)/\ell \\ \mathbf{S}(\mathbf{p}_Q - \mathbf{p}_L)(\mathbf{v}_Q - \mathbf{v}_L)/\ell^2 \end{bmatrix}, \quad (2)$$

where $\Omega_{\mathbf{x}} := \mathbb{R}^3 \times \mathbb{R}^3 \times \mathbf{S}^2 \times \mathbb{R}^3$, $\mathbf{n}$ and $\boldsymbol{\omega}$ are direction vector and angular velocity of the cable, and $\mathbf{p}_d$ is a feasible trajectory given in *Definition* 1.

By applying Newton's second law to both the quadrotor and the load, we obtain

$$m_Q \dot{\mathbf{v}}_Q = -T\mathbf{r} - T_L\mathbf{n} + m_Q g\mathbf{e}_3 + \mathbf{d}_Q, \quad (3)$$
$$m_L \dot{\mathbf{v}}_L = T_L\mathbf{n} + m_L g\mathbf{e}_3 + \mathbf{d}_L, \quad (4)$$

where $\mathbf{d}_{L/Q} \in \mathbb{R}^3$ are time-varying lumped terms containing both internal parametric uncertainty and external disturbances; $m_{L/Q}$ are the masses of the load/quadrotor; g is the acceleration of gravity; $\mathbf{e}_3 := [0,\ 0,\ 1]^\mathsf{T}$; and $T_L \in \mathbb{R}_{\geq 0}$ is the tension in the cable. By substituting the second time derivative of $\mathbf{n}$ into the difference between (3) and (4), we have $T_L = (m_L/(m_L+m_Q))[m_Q\ell\|\boldsymbol{\omega}\|^2 - (T\mathbf{r} - \mathbf{d}_Q + (m_Q/m_L)\mathbf{d}_L)^\mathsf{T}\mathbf{n}]$. Furthermore, from (3)-(4), the $\mathbf{y}$ system state is governed by

$$\dot{\mathbf{y}} := f_{\mathbf{y}}(\mathbf{y},\ \mathbf{u}_{\mathbf{y}}) = [\mathbf{v}_Q^\mathsf{T}, \mathbf{v}_L^\mathsf{T}, \dot{\mathbf{v}}_Q^\mathsf{T}, \dot{\mathbf{v}}_L^\mathsf{T}]^\mathsf{T}. \quad (5)$$

Similar to a typical quadrotor system, we define the control input to the $\mathbf{x}$ system as $\mathbf{u}_{\mathbf{x}} := [T_{\mathbf{x}},\ \boldsymbol{\tau}_{\mathbf{x}}^\mathsf{T}]^\mathsf{T} \in \mathbb{R}^4$, where $T_{\mathbf{x}}$ and $\boldsymbol{\tau}_{\mathbf{x}}$ denote desired tension and torque on the cable, respectively. The transformation rule of control inputs is defined as

$$\mathbf{u}_{\mathbf{y}}(\mathbf{u}_{\mathbf{x}},\ \mathbf{r}) := \left[-\mathcal{F}_{\mathbf{x}}^\mathsf{T}\mathbf{r},\ \mathbf{r}^\mathsf{T}\right]^\mathsf{T} \in \mathbb{R}^4, \quad (6)$$

where $\mathcal{F}_{\mathbf{x}} \in (\Omega_{\mathbf{x}} \times \mathbb{R}^4,\ \mathbb{R}^3)$ is an equivalent control input, defined as

$$\mathcal{F}_{\mathbf{x}} := \left(\frac{m_Q + m_L}{m_L} T_{\mathbf{x}} - m_Q\ell\|\boldsymbol{\omega}\|^2\right)\mathbf{n} + m_Q\ell\boldsymbol{\Pi}(\mathbf{n})\boldsymbol{\tau}_{\mathbf{x}}, \quad (7)$$

and where $\|\mathcal{F}_{\mathbf{x}}\| \neq 0$ is elaborated later in Section V. From the above, the $\mathbf{x}$ system state in (2) is governed by

$$\dot{\mathbf{x}} := h_{\mathbf{x}}(\mathbf{x},\ \mathbf{u}_{\mathbf{x}}) = \begin{bmatrix} \mathbf{e}_v \\ \frac{T_{\mathbf{x}}\mathbf{n}}{m_L} + g\mathbf{e}_3 - \ddot{\mathbf{p}}_d + \boldsymbol{\Delta}_{L_x} \\ \mathbf{S}(\boldsymbol{\omega})\mathbf{n} \\ \mathbf{S}(\mathbf{n})\boldsymbol{\tau}_{\mathbf{x}} + \boldsymbol{\Delta}_{C_x} \end{bmatrix}, \quad (8)$$

with the lumped uncertainties defined as

$$\boldsymbol{\Delta}_{L_x} := \frac{\mathbf{d}_L}{m_L} - \frac{m_Q\mathbf{n}\mathbf{n}^\mathsf{T}\mathbf{d}_L}{m_L(m_Q+m_L)} + \frac{\mathbf{n}\mathbf{n}^\mathsf{T}\mathbf{d}_Q}{m_Q+m_L} - \frac{\mathbf{n}\mathbf{n}^\mathsf{T}\boldsymbol{\Pi}(\mathbf{r})\mathcal{F}_{\mathbf{x}}}{m_L+m_Q},$$
$$\boldsymbol{\Delta}_{C_x} := -\frac{\mathbf{S}(\mathbf{n})\mathbf{d}_L}{m_L\ell} + \frac{\mathbf{S}(\mathbf{n})\mathbf{d}_Q}{m_Q\ell} - \frac{\mathbf{S}(\mathbf{n})\boldsymbol{\Pi}(\mathbf{r})\mathcal{F}_{\mathbf{x}}}{m_Q\ell}.$$

Definition 1: We consider the desired trajectory for the load $\mathbf{p}_d \in \mathcal{C}^5(\mathbb{R}_{\geq 0})$ as a feasible trajectory if: i) $\sup_{t\geq 0}\|\mathbf{p}_d^{(i)}\| < \infty$ for $i \in \{2,\ 3,\ 4\}$, ii) $\sup_{t\geq 0}\|\mathbf{e}_3^\mathsf{T}\ddot{\mathbf{p}}_d\| > -g$, and iii) $\inf_{t\geq 0}\mathcal{P}(t) < 1$, with

$$\mathcal{P}(t) := \frac{m_Q}{m_L(m_Q+m_L)} \frac{\ell\|\mathbf{S}(\check{\mathbf{n}})\mathbf{p}_d^{(3)}(t)\|^2}{\|-g\mathbf{e}_3 + \ddot{\mathbf{p}}_d(t)\|^3},$$

where $\check{\mathbf{n}} := (-g\mathbf{e}_3 + \ddot{\mathbf{p}}_d)/\|g\mathbf{e}_3 - \ddot{\mathbf{p}}_d\|$.

Problem 1: Consider the feasible trajectory of the load $\mathbf{p}_d$. For the given system (5), the prescribed trajectory $\mathbf{p}_d$, and a given positive constant ε_e, we design the control input $\mathbf{u}_{\mathbf{y}}$, such that $\lim_{t\to\infty}\|\mathbf{p}_L(t) - \mathbf{p}_d(t)\| \leq \varepsilon_e$.

Remark 1: Since the cable lacks actuation, we cannot directly design the actual tension T_L. Rather, we specify the desired value $T_{\mathbf{x}}$ in the $\mathbf{x}$ system, subsequently obtaining the thrust force $-T\mathbf{r}$ in the $\mathbf{y}$ system, which comprises two orthogonal forces $T_{\mathbf{x}}\mathbf{n}$ and $\boldsymbol{\Pi}(\mathbf{n})\boldsymbol{\tau}_{\mathbf{x}}$. Moreover, this control approach obviates the need to measure the tension value.

Remark 2: The motivation behind introducing the $\mathbf{x}$ system is to align the dynamics of the QSLS in (5) with those of a typical quadrotor system, enabling the direct application of various existing control methods for quadrotors to the QSLS. The coordinate transformation strategy, as depicted in Fig. 3, ensures straightforward conversions of states $\mathbf{y}$ to $\mathbf{x}$ and control inputs $\mathbf{u}_{\mathbf{x}}$ to $\mathbf{u}_{\mathbf{y}}$.

IV. CONTROLLER DESIGN

As illustrated in Fig. 3, we shall start by designing control inputs $T_{\mathbf{x}}$ and $\boldsymbol{\tau}_{\mathbf{x}}$ to the $\mathbf{x}$ system to control the translational subsystem $(\mathbf{p}_L, \mathbf{v}_L)$ and the attitude subsystem $(\mathbf{n},\ \boldsymbol{\omega})$, respectively. Subsequently, we utilize the control input transformation (6) and (7) to transfer the input $\mathbf{u}_{\mathbf{x}}$ to the input $\mathbf{u}_{\mathbf{y}}$ for the $\mathbf{y}$ system and generate the desired quadrotor attitude $\mathbf{r}_d$.

A. Load Position Controller Design

With the purpose of driving the position and velocity errors of the load to zero, we consider a Lyapunov function candidate $V_1 := (1/2)\mathbf{e}_p^\mathsf{T}\mathbf{e}_p + (1/2)\mathbf{e}^\mathsf{T}\mathbf{e}$, where the coupling error $\mathbf{e}$ is defined as $\mathbf{e} := k_p\mathbf{e}_p + \mathbf{e}_v$, and where k_p is a

positive control gain. Substituting (8) into the time derivative of V_1, and adding and subtracting $\mathbf{e}_p^\mathsf{T}\mathbf{e}$, yield

$$\dot{V}_1 = \mathbf{e}^\mathsf{T}(\mathbf{e}_p + k_p\mathbf{e}_v + \frac{T_\mathbf{x}\mathbf{n}}{m_{_L}} + g\mathbf{e}_3 - \ddot{\mathbf{p}}_d + \boldsymbol{\Delta}_{_{Lx}}) - k_p\|\mathbf{e}_p\|^2 \quad (9)$$

To relieve the constraint that the actuation force $T_\mathbf{x}\mathbf{n}$ in (9) is always aligned with the direction $\mathbf{n}$, we introduce a virtual control input $\mathbf{F}_{\mathbf{x}_d} \in \mathbb{R}^3$ such that

$$T_\mathbf{x} := \mathbf{n}^\mathsf{T}\mathbf{F}_{\mathbf{x}_d}, \quad (10)$$

and lump its component perpendicular to $\mathbf{n}$ into uncertainties $\boldsymbol{\Delta}_{_L}$, with the representations

$$T_\mathbf{x}\mathbf{n} = \mathbf{F}_{\mathbf{x}_d} - \boldsymbol{\Pi}(\mathbf{n})\mathbf{F}_{\mathbf{x}_d}, \quad (11)$$

$$\boldsymbol{\Delta}_{_L} := \boldsymbol{\Delta}_{_{Lx}} - \frac{\boldsymbol{\Pi}(\mathbf{n})\mathbf{F}_{\mathbf{x}_d}}{m_{_L}}. \quad (12)$$

Integrating (11) and (12) into (9), adding and subtracting $k_2\mathbf{e}^\mathsf{T}\mathbf{e}$, the time derivative $\dot{V}_1$ can be rewritten as $\dot{V}_1 = -k_p\|\mathbf{e}_p\|^2 - k_2\|\mathbf{e}\|^2 + \mathbf{e}^\mathsf{T}(\mathbf{F}_{\mathbf{x}_d}/m_{_L} + g\mathbf{e}_3 - \ddot{\mathbf{p}}_d + \mathbf{e}_p + k_p\mathbf{e}_v + k_2\mathbf{e} + \boldsymbol{\Delta}_{_L})$, where k_2 is a positive gain.

Now, from the expression of $\dot{V}_1$, we define the virtual control input $\mathbf{F}_{\mathbf{x}_d}$ as

$$\mathbf{F}_{\mathbf{x}_d} := -m_{_L}\left[\mathbf{e}_p + k_p\mathbf{e}_v + k_2\mathbf{e} + g\mathbf{e}_3 - \ddot{\mathbf{p}}_d + \widehat{\boldsymbol{\Delta}}_{_L}\right], \quad (13)$$

where $\widehat{\boldsymbol{\Delta}}_{_L}$ is the estimate of $\boldsymbol{\Delta}_{_L}$, given by

$$\widehat{\boldsymbol{\Delta}}_{_L} := g_{_L}(t) \otimes \boldsymbol{\Delta}_{_L}, \quad (14)$$

and where $g_{_L}(t) \in \mathbb{R}$ is the impulse response of the filter $\mathcal{G}_{_L}(s) = k_{_L}/(s + k_{_L}) \in \mathbb{R}$ with a positive filter gain $k_{_L}$. Combining (13) and (14), the completed UDE-based robust control input at the translational level is formulated as

$$\mathbf{F}_{\mathbf{x}_d} = m_{_L}\left[\ddot{\mathbf{p}}_d - g\mathbf{e}_3 - \mathcal{L}^{-1}\left(\frac{s\mathcal{G}_{_L}(s)}{1-\mathcal{G}_{_L}(s)}\right)\mathbf{e}_v - \mathcal{L}^{-1}\left(\frac{1}{1-\mathcal{G}_{_L}(s)}\right)(\mathbf{e}_p + k_p\mathbf{e}_v + k_2\mathbf{e})\right]. \quad (15)$$

According to (12), $\boldsymbol{\Delta}_{_L}$ is an unknown vector, which cannot be directly measured. Therefore, we introduce an equivalence

$$\boldsymbol{\Delta}_{_L} = \dot{\mathbf{e}}_v + \ddot{\mathbf{p}}_d - \frac{\mathbf{F}_{\mathbf{x}_d}}{m_{_L}} - g\mathbf{e}_3, \quad (16)$$

obtained from (8). Substituting (16) into (14), and introducing an auxiliary variable $\varpi_{_L}$, the realization of $\widehat{\boldsymbol{\Delta}}_{_L}$, in time domain, follows as $\dot{\varpi}_{_L} = -k_{_L}\varpi_{_L} - k_{_L}(\mathbf{e}_v + \dot{\mathbf{p}}_{_{Ld}}) - \mathbf{F}_{\mathbf{x}_d}/m_{_L} - g\mathbf{e}_3$ and $\widehat{\boldsymbol{\Delta}}_{_L} = \mathbf{e}_v + \dot{\mathbf{p}}_{_{Ld}} - \varpi_{_L}$.

B. Cable Attitude Controller Design

To proceed, we define the cable direction error as $\mathbf{e}_n := \mathbf{n} - \mathbf{n}_d$, where $\mathbf{n}_d := \mathbf{F}_{\mathbf{x}_d}/\|\mathbf{F}_{\mathbf{x}_d}\|$ is the desired values of $\mathbf{n}$. To drive the cable direction error to zero, the third tentative Lyapunov function candidate is constructed as $V_2 := (1/2)\mathbf{e}_n^\mathsf{T}\mathbf{e}_n$ with the time derivative given by $\dot{V}_2 = \mathbf{n}_d^\mathsf{T}\mathbf{S}(\mathbf{n})(\boldsymbol{\omega} - \boldsymbol{\omega}_{\mathbf{n}_d})$, where $\boldsymbol{\omega}_{\mathbf{n}_d}$, the corresponding angular velocity with respect to $\mathbf{n}_d$, is defined as $\boldsymbol{\omega}_{\mathbf{n}_d} := \mathbf{S}(\mathbf{n}_d)\dot{\mathbf{F}}_{\mathbf{x}_d}/\|\mathbf{F}_{\mathbf{x}_d}\|$. Following the backstepping procedure, to incorporate a negative term $k_n\|\boldsymbol{\Pi}(\mathbf{n})\mathbf{e}_n\|^2$ associated with the error $\mathbf{e}_n$, the time derivative $\dot{V}_2$ is updated as $\dot{V}_2 = -k_n\|\boldsymbol{\Pi}(\mathbf{n})\mathbf{e}_n\|^2 + \mathbf{n}_d^\mathsf{T}\mathbf{S}(\mathbf{n})(\boldsymbol{\omega} - \boldsymbol{\omega}_d)$, where, k_n is a positive control gain, and $\boldsymbol{\omega}_d := \boldsymbol{\omega}_{\mathbf{n}_d} + k_n\mathbf{S}(\mathbf{n})\mathbf{n}_d$.

To simplify the mathematical presentation, we define the cable angular velocity error as $\mathbf{e}_\omega := \mathbf{S}(\mathbf{n})(\boldsymbol{\omega} - \boldsymbol{\omega}_d)$. The fourth Lyapunov function candidate is augmented with the defined error $\mathbf{e}_\omega$ as $V_3 := V_2 + (1/2)\mathbf{e}_\omega^\mathsf{T}\mathbf{e}_\omega$, where its time derivative yields

$$\dot{V}_3 = -k_n\|\boldsymbol{\Pi}(\mathbf{n})\mathbf{e}_n\|^2 + \mathbf{e}_\omega^\mathsf{T}(\dot{\mathbf{e}}_\omega + \mathbf{n}_d). \quad (17)$$

Substituting (8) into (18), adding and subtracting $k_\omega\|\mathbf{e}_\omega\|^2$, $\dot{V}_3$ is rewritten as

$$\dot{V}_3 = -k_n\|\boldsymbol{\Pi}(\mathbf{n})\mathbf{e}_n\|^2 - k_\omega\|\mathbf{e}_\omega\|^2 + \mathbf{e}_\omega^\mathsf{T}[-\boldsymbol{\Pi}(\mathbf{n})\boldsymbol{\tau}_\mathbf{x} - \mathbf{S}(\mathbf{n})\dot{\boldsymbol{\omega}}_d + \mathbf{S}(\dot{\mathbf{n}})(\boldsymbol{\omega} - \boldsymbol{\omega}_d) + \mathbf{n}_d + k_\omega\mathbf{e}_\omega + \boldsymbol{\Delta}_{_C}], \quad (18)$$

where k_ω is a positive control gain, and

$$\boldsymbol{\Delta}_{_C} := \mathbf{S}(\mathbf{n})\boldsymbol{\Delta}_{_{Cx}} = \mathbf{S}(\mathbf{n})\dot{\boldsymbol{\omega}} + \boldsymbol{\tau}_\mathbf{x}. \quad (19)$$

Similar to $\mathbf{F}_{\mathbf{x}_d}$ in (25), from the expression of $\dot{V}_3$, we define the control input $\boldsymbol{\tau}_\mathbf{x}$ at the rotational level as

$$\boldsymbol{\tau}_\mathbf{x} := \mathcal{L}^{-1}\left(\frac{1}{1-\mathcal{G}_{_C}(s)}\right)(\mathbf{S}(\dot{\mathbf{n}})(\boldsymbol{\omega} - \boldsymbol{\omega}_d) - \mathbf{S}(\mathbf{n})\dot{\boldsymbol{\omega}}_d + k_n\mathbf{n}_d + k_\omega\mathbf{e}_\omega) + \mathbf{S}(\mathbf{n})\mathcal{L}^{-1}\left(\frac{s\mathcal{G}_{_C}(s)}{1-\mathcal{G}_{_C}(s)}\right)\boldsymbol{\omega}, \quad (20)$$

where the filter $\mathcal{G}_{_C}(s) = k_{_C}/(s + k_{_C}) \in \mathbb{R}$ with $k_{_C} \in \mathbb{R}_{>0}$ is used to compensate for the perturbation caused by $\boldsymbol{\Delta}_{_C}$.

C. Quadrotor Attitude Controller Design

The objective of this section is to drive the direction $-\mathbf{r}$ of the thrust force to a desired direction $-\mathbf{r}_d$ which in line with equation (7), is set as $\mathbf{r}_d := -\mathcal{F}_\mathbf{x}(\mathbf{x}, \mathbf{u}_\mathbf{x})/\|\mathcal{F}_\mathbf{x}(\mathbf{x}, \mathbf{u}_\mathbf{x})\|$. We introduce the quadrotor attitude error as $\mathbf{e}_r := \mathbf{r} - \mathbf{r}_d$ and a Lyapunov function candidate $V_4 := (1/2)\mathbf{e}_r^\mathsf{T}\mathbf{e}_r$ with its time derivative given by $\dot{V}_4 = \mathbf{r}_d^\mathsf{T}\mathbf{R}\mathbf{S}(\mathbf{e}_3)\left[\boldsymbol{\omega}_{_Q} - \mathbf{R}^\mathsf{T}\mathbf{S}(\mathbf{r}_d)\dot{\mathbf{r}}_d\right]$. Due to the existence of the estimation errors $\widetilde{\boldsymbol{\Delta}}_{_L} := \boldsymbol{\Delta}_{_L} - \widehat{\boldsymbol{\Delta}}_{_L}$ and $\widetilde{\boldsymbol{\Delta}}_{_C} := \boldsymbol{\Delta}_{_C} - \widehat{\boldsymbol{\Delta}}_{_C}$, consider the expression $\dot{\mathbf{r}}_d := \dot{\mathbf{r}}_{d_n} + (\partial\mathbf{r}_d/\partial\mathbf{v}_{_L})\widetilde{\boldsymbol{\Delta}}_{_L} + (\partial\mathbf{r}_d/\partial\boldsymbol{\omega})\widetilde{\boldsymbol{\Delta}}_{_C}$, where $\dot{\mathbf{r}}_{d_n}$ represents the nominal part of $\dot{\mathbf{r}}_d$ computed at $\widehat{\boldsymbol{\Delta}}_{_L} = \boldsymbol{\Delta}_{_L}$ and $\widehat{\boldsymbol{\Delta}}_{_C} = \boldsymbol{\Delta}_{_C}$.

From the expression of $\dot{V}_4$, the angular velocity of the quadrotor $\boldsymbol{\omega}_{_Q}$ is designed as

$$\boldsymbol{\omega}_{_Q} := \boldsymbol{\Pi}(\mathbf{e}_3)\left[\mathbf{R}^\mathsf{T}\mathbf{S}(\mathbf{r}_d)\dot{\mathbf{r}}_{d_n} + k_{\omega_Q}\mathbf{S}(\mathbf{e}_3)\mathbf{R}^\mathsf{T}\mathbf{r}_d\right] - k_\psi(\psi - \psi_d)\mathbf{e}_3, \quad (21)$$

where $k_{\omega_Q} \in \mathbb{R}_{>0}$ and $k_\psi \in \mathbb{R}_{>0}$ are control gains, and ψ and ψ_d are respectively the actual and desired yaw angles of the quadrotor.

Remark 3: The uncertainties $\boldsymbol{\Delta}_{_L}$ in (12) and $\boldsymbol{\Delta}_{_C}$ in (19) are functions of the external disturbances $\mathbf{d}_{_{L/Q}}$ and tracking errors rather than control forces $\mathbf{F}_{\mathbf{x}_d}$ and $\mathcal{F}_\mathbf{x}$.

V. GLOBAL SYSTEM ANALYSIS

Theorem 1: Consider the feasible trajectory $\mathbf{p}_d(t)$, and the state $\mathbf{x}(t)$ with $\dot{\mathbf{x}}(t) = h_{\mathbf{x}}(t, \mathbf{x}, \mathbf{u}_{\mathbf{x}}(t, \mathbf{x}))$ in (8). For $\forall t > 0$, provided that the state $\mathbf{x}(t)$ satisfies $\|\mathbf{x}(t) - \check{\mathbf{x}}(t)\| \leq \epsilon$ with an arbitrary positive number ϵ, then $\inf_{t\geq 0} \|\mathcal{F}_{\mathbf{x}}(\mathbf{x}, \mathbf{u}_{\mathbf{x}})\| > 0$.

Proof: From the definition of $T_{\mathbf{x}}$ in (10), one can conclude that $\sup_{t\geq 0} \max \|\partial T_{\mathbf{x}}(t, \mathbf{x})/\partial \mathbf{x}\| \leq \bar{T}_{\mathbf{x}} \in \mathbb{R}_{>0}$ is bounded when the error states $\mathbf{e}$ and $\mathbf{e}_v$ are bounded. We then introduce a standard vector $T_{\mathbf{x}}(t, \check{\mathbf{x}}) := \|g\mathbf{e}_3 - \ddot{\mathbf{p}}_d\|$ in $\check{\mathbf{x}}$ system whose states are known, where $\check{\mathbf{x}}$ system represents the nominal $\mathbf{x}$ system computed at that all tracking errors are zero. Employing the Lagrange's Mean Value Theorem, yields

$$\|T_{\mathbf{x}}(t, \mathbf{x}) - T_{\mathbf{x}}(t, \check{\mathbf{x}})\| \leq \max_{\|\mathbf{x}-\check{\mathbf{x}}(t)\|\leq\epsilon} \left\| \frac{\partial T_{\mathbf{x}}(t, \mathbf{x})}{\partial \mathbf{x}} \right\| \|\mathbf{x}(t) - \check{\mathbf{x}}(t)\|$$
$$\implies \sup_{t\geq 0} \|T_{\mathbf{x}}(t, \mathbf{x}) - T_{\mathbf{x}}(t, \check{\mathbf{x}})\| \leq \bar{T}_{\mathbf{x}}\epsilon. \tag{22}$$

Now, $\mathcal{F}_{\mathbf{x}}(\mathbf{x}, \mathbf{u}_{\mathbf{x}})$ in equation (7), with the property established in (22), verifies

$$\|\mathcal{F}_{\mathbf{x}}(\mathbf{x}, \mathbf{u}_{\mathbf{x}}(t, \mathbf{x})\| \geq \; |(m_Q + m_L)T_{\mathbf{x}}(t, \check{\mathbf{x}}) - m_Q l\|\check{\boldsymbol{\omega}}\|^2 - \epsilon \left(m_Q l(\epsilon + 2\check{\boldsymbol{\omega}}_s) + (m_Q + m_L)\bar{T}_{\mathbf{x}}\right)|, \tag{23}$$

where $\check{\boldsymbol{\omega}} := \mathbf{S}(\check{\mathbf{n}})\mathbf{p}_d^{(3)}/\|g\mathbf{e}_3 - \ddot{\mathbf{p}}_d\|$ and $\check{\boldsymbol{\omega}}_s := \sup_{t\geq 0} \|\check{\boldsymbol{\omega}}(t)\| < \infty$. From *Definition* 1 and (23), one can conclude that given $\|\mathbf{x}(t) - \check{\mathbf{x}}(t)\| \leq \epsilon$, $\mathcal{F}_{\mathbf{x}}(\mathbf{x}, \mathbf{u}_{\mathbf{x}})$ satisfies $\inf_{t\geq 0} \|\mathcal{F}_{\mathbf{x}}\| > 0$. ■

According to *Theorem* 1, if $\mathbf{p}_d$ is a feasible trajectory, we have that $\inf_{t\geq 0} \|\mathcal{F}_{\mathbf{x}}(\check{\mathbf{x}}, \mathbf{u}_{\check{\mathbf{x}}})\| > 0$ and $\mathbf{u}_{\mathbf{y}}$ in (6) is well defined with $\mathcal{F}_{\mathbf{x}}(\check{\mathbf{x}}, \mathbf{u}_{\check{\mathbf{x}}}) \neq 0$, which implies that for any state $\mathbf{x}(t)$, there always exists the corresponding control input $\mathbf{u}_{\mathbf{y}}$.

By substituting (6) and (7) into the tension T_L, we obtain $T_L = T_{\mathbf{x}} + \mathbf{n}^{\mathsf{T}}(m_L\boldsymbol{\Delta}_{L_x} - \mathbf{d}_L)$. From *Definition* 1, the tension $T_L(\check{\mathbf{x}})$ in $\check{\mathbf{x}}$ system is always positive. Similar to the proof of *Theorem* 1, one can conclude that given $\|\mathbf{x}(t) - \check{\mathbf{x}}(t)\| \leq \epsilon$, the tension in cable satisfies $\inf_{t\geq 0} T_L > 0$.

Theorem 2: Consider the feasible trajectory $\mathbf{p}_d$, the estimates $\widehat{\boldsymbol{\Delta}}_L$ and $\widehat{\boldsymbol{\Delta}}_C$, and the $\mathbf{x}$ system described in (8), in closed-loop with the control laws given in (10), (20), and (21). For the any initial state $\mathbf{x}(0)$, the tracking and estimation errors $\mathbf{e}_p$, $\mathbf{e}$, $\mathbf{e}_n$, $\mathbf{e}_\omega$, $\mathbf{e}_r$, $\widetilde{\boldsymbol{\Delta}}_L$, and $\widetilde{\boldsymbol{\Delta}}_C$ are UUB.

Proof: We consider a Lyapunov function candidate consisting of estimation errors $\widetilde{\boldsymbol{\Delta}}_L$ and $\widetilde{\boldsymbol{\Delta}}_C$ as $V_\Delta := \widetilde{\boldsymbol{\Delta}}_L^{\mathsf{T}}\widetilde{\boldsymbol{\Delta}}_L/2 + \widetilde{\boldsymbol{\Delta}}_C^{\mathsf{T}}\widetilde{\boldsymbol{\Delta}}_C/2$. From the design of the estimate $\widehat{\boldsymbol{\Delta}}_L$ in (14), the realization of $\widehat{\boldsymbol{\Delta}}_L$ in frequency domain verifies $s\widehat{\boldsymbol{\Delta}}_L(s) = k_L\widetilde{\boldsymbol{\Delta}}_L(s)$, leading to $\dot{\widehat{\boldsymbol{\Delta}}}_L(t) = k_L\widetilde{\boldsymbol{\Delta}}_L(t)$. Employing the above, the time derivative of V_Δ satisfies $\dot{V}_\Delta \leq \zeta_{\Delta_L}\|\widetilde{\boldsymbol{\Delta}}_L\| - k_L\|\widetilde{\boldsymbol{\Delta}}_L\|^2 + \zeta_{\Delta_C}\|\widetilde{\boldsymbol{\Delta}}_C\| - k_C\|\widetilde{\boldsymbol{\Delta}}_C\|^2$, where $\zeta_{\Delta_L} := \sup_{t>0} \|\dot{\boldsymbol{\Delta}}_L\|$ and $\zeta_{\Delta_C} := \sup_{t>0} \|\dot{\boldsymbol{\Delta}}_C\|$.

We further consider the final Lyapunov function $V := V_1 + V_2 + V_3 + V_4 + V_\Delta$, with its time derivative $\dot{V}$ given by

$$\begin{aligned}\dot{V} \leq & -k_p\|\mathbf{e}_p\|^2 - k_2\|\mathbf{e}\|^2 + \|\mathbf{e}\|\|\widetilde{\boldsymbol{\Delta}}_L\| - k_n\|\boldsymbol{\Pi}(\mathbf{n})\mathbf{e}_n\|^2 \\ & - k_\omega\|\mathbf{e}_\omega\|^2 + \|\mathbf{e}_\omega\|\|\widetilde{\boldsymbol{\Delta}}_C\| - k_{\omega_Q}\|\boldsymbol{\Pi}(\mathbf{r})\mathbf{e}_r\|^2 \\ & + \|\boldsymbol{\Pi}(\mathbf{r})\mathbf{e}_r\| \left(\zeta_{r_L}\|\widetilde{\boldsymbol{\Delta}}_L\| + \zeta_{r_C}\|\widetilde{\boldsymbol{\Delta}}_C\|\right) + \zeta_{\Delta_L}\|\widetilde{\boldsymbol{\Delta}}_L\| \\ & - k_L\|\widetilde{\boldsymbol{\Delta}}_L\|^2 + \zeta_{\Delta_C}\|\widetilde{\boldsymbol{\Delta}}_C\| - k_C\|\widetilde{\boldsymbol{\Delta}}_C\|^2,\end{aligned} \tag{24}$$

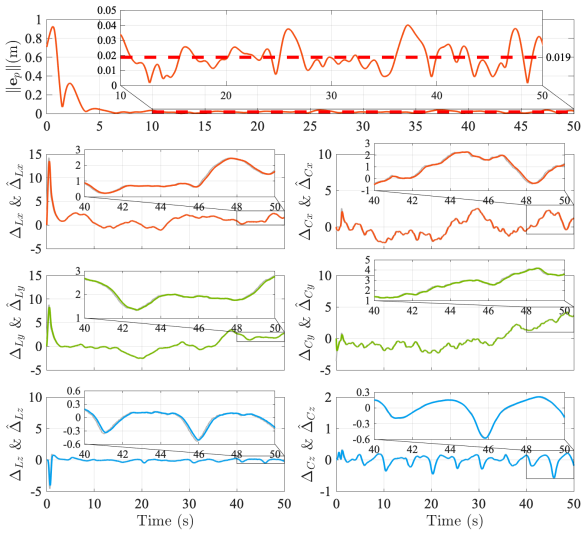

Fig. 4. Time evolution of the position error, disturbances and its estimates.

where $\zeta_{r_L} := \sup_{t>0} \|\partial \mathbf{r}_d/\partial \mathbf{v}_L\|$ and $\zeta_{r_C} := \sup_{t>0} \|\partial \mathbf{r}_d/\partial \boldsymbol{\omega}\|$. Employing Young's inequality, $\dot{V}$ in (24) can be rewritten as

$$\dot{V} \leq -\alpha\|\mathbf{z}\|^2 + \Lambda, \tag{25}$$

where $\mathbf{z} := [\mathbf{e}_p^{\mathsf{T}}, \mathbf{e}^{\mathsf{T}}, \boldsymbol{\Pi}(\mathbf{n})\mathbf{e}_n^{\mathsf{T}}, \mathbf{e}_\omega^{\mathsf{T}}, \boldsymbol{\Pi}(\mathbf{r})\mathbf{e}_r^{\mathsf{T}}, \widetilde{\boldsymbol{\Delta}}_L^{\mathsf{T}}, \widetilde{\boldsymbol{\Delta}}_C^{\mathsf{T}}]^{\mathsf{T}} \in \mathbb{R}^{21}$ is the cascaded error, $\alpha := \min\{k_p,\ k_2 - \lambda_v/2,\ k_n,\ k_\omega - \lambda_\omega/2,\ k_{\omega_Q} - \lambda_{r_L}\zeta_{r_L}/2 - \lambda_{r_C}\zeta_{r_C}/2,\ k_L - 1/(2\lambda_v) - \zeta_{r_L}/(2\lambda_{r_L}) - \zeta_{\Delta_L}/(2\lambda_{\Delta_L}),\ k_C - 1/(2\lambda_\omega) - \zeta_{r_C}/(2\lambda_{r_C}) - \zeta_{\Delta_C}/(2\lambda_{\Delta_C})\} \in \mathbb{R}_{>0}$ with positive constants λ_ω, λ_{r_L}, λ_{r_C}, λ_{Δ_L}, and λ_{Δ_C}, and the positive number $\Lambda := \lambda_{\Delta_L}\zeta_{\Delta_L}/2 + \lambda_{\Delta_C}\zeta_{\Delta_C}/2$. According to (25), the cascaded error $\mathbf{z}$ is UUB with the ultimate bound given by $\|\mathbf{z}\| \leq \sqrt{\Lambda/\alpha}$, resulting in $V \leq \Lambda/(2\alpha)$ (from the definition $V = \|\mathbf{z}\|^2/2$). ■

The essence of *Theorem* 2 is that, with feasible trajectories and under the proposed controller, the errors of the transformed system $\mathbf{x}$ ultimately converge to a region surrounding zero. Based on the *Theorems* 1 and 2, there exists a number $\epsilon_e \in \mathbb{R}_{>0}$ satisfying $\lim_{t\to\infty} \|\mathbf{p}_L(t) - \mathbf{p}_d(t)\| \leq \varepsilon_e$, which means that *Problem* 1 is addressed.

Remark 4: When the disturbances $\mathbf{d}_{L/Q}$ in (3) and (4) are zero, the lumped uncertainties $\boldsymbol{\Delta}_L$ in (12) and $\boldsymbol{\Delta}_C$ in (19) become functions of the tracking errors, ensuring $\zeta_{\Delta_{L/C}} = 0$ and $\Lambda = 0$. In such case, the time derivative in (25) satisfies $\dot{V} \leq -\alpha\|\mathbf{z}\|^2$. With the feasible trajectory $\mathbf{p}_d$, all terms of the time derivative of $\dot{V}$ are bounded, from which it follows that $\dot{V}$ is uniformly continuous. We can now invoke Barbalat's Lemma to infer the convergence of $\dot{V}$ to zero, resulting in the convergence of tracking errors to zero. Consequently, the lumped uncertainties $\boldsymbol{\Delta}_{L/C}$ also converge to zero.

VI. SIMULATION RESULTS

This section presents simulation results in a MATLAB/Simulink environment to validate the convergence performance and the robustness of the proposed controller. The length of the cable used in the simulation is $\ell = 0.6$ m, the quadrotor mass is $m_Q = 0.21$ kg and the load mass

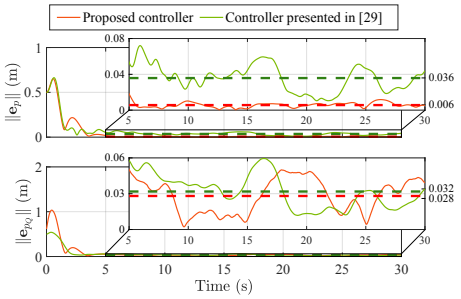

Fig. 5. Time evolution of the position error of the load and the quadrotor.

is $m_{_L} = 0.05$ kg. Consider a reference spherical Lissajous curve described by the following parametric vector:

$$\mathbf{p}_d(\gamma(t)) := \begin{bmatrix} \sin(\gamma(t))\cos(\gamma(t)-\pi) \\ \sin(\gamma(t))\sin(\gamma(t)-\pi) \\ \cos(\gamma(t)) \end{bmatrix} \text{ (m)}, \qquad (26)$$

where $\gamma(t) \in \mathbb{R}$ is a pseudo-velocity parameter defined as $\gamma(t) := v_d \int_0^t \|\partial \mathbf{p}_d(\gamma(\tau))/\partial\gamma(\tau)\|^{-1} d\tau$. such that the speed along the trajectory is v_d.

We considered disturbances characterized by a Brownian motion, more specifically, described by the following differential equations $\dot{\mathbf{d}}_{_{L/Q}} = [-\mathbf{d}_{_{L/Q}} + \mathbf{a}_{_{L/Q}} \odot \mathbf{w_d}] \oslash [16.5, 15, 19]$, where gain matrices $\mathbf{a}_{_L} = [1.6, 1.5, 2.2]$ and $\mathbf{a}_{_Q} = [3.2, 3, 4.4]$, and $\mathbf{w}_\mathrm{d} \in \mathbb{R}^3$ is a vector of zero-mean Gaussian noise sequences produced from various seeds, with noise power set to 10^{-3}. The simulation starts with the load and the quadrotor initially at rest at $\mathbf{p}_{_L}(0) = [0.5,\ 0,\ -1]^\mathsf{T}$m, and with $\mathbf{v}_{_L}(0) = [0,\ 0,\ 0]^\mathsf{T}$m/s, $\mathbf{n}(0) = [0,\ 0,\ -1]^\mathsf{T}$, $\boldsymbol{\omega}(0) = [0,\ 0,\ 0]^\mathsf{T}$rad/s, and the quadrotor orientation $\mathbf{R}(0) = \mathbf{I}_3$. The control gains used in simulation results were $k_p = 1$, $k_2 = 1$, $k_n = 2$, $k_\omega = 2$, $k_\psi = 2$, $k_{\omega_Q} = 4$, $k_{_L} = 10$, and $k_{_C} = 10$.

The effectiveness of the proposed control strategy is demonstrated through the results of tracking the reference (26) presented in Fig. 4. During steady-state operation, the position error converges to a mean value of approximately 1.9 cm, as illustrated in Fig. 4. Furthermore, the proposed methodology exhibits robustness to time-varying lumped disturbances, as demonstrated by the convergence of the disturbance estimates to their corresponding actual values over the entire maneuver.

In addition, a simulation comparison between the proposed controller and the controller presented in [29] is analyzed. We selected the line trajectory $\mathbf{p}_d := [0,\ t,\ -1]^\mathsf{T}$(m) and used the time-varying disturbances to ensure fairness in the comparisons, with results shown in Fig. 5. Although in steady-state, the mean magnitudes of the quadrotor position error $\|\mathbf{e}_{pQ}\|$ resulting from the proposed controller and the controller in [29] are very close (2.8 cm and 3.2 cm, respectively), the load position error $\|\mathbf{e}_p\|$ exhibits a significant difference (0.6 cm for the proposed controller and 3.6 cm for [29], respectively).

VII. EXPERIMENTAL RESULTS

Due to the lack of payload for onboard sensors, the states of the quadrotor were measured through external sensors. The indoors drone-testing arena in the SCORE Laboratory of the University of Macau is an $11 \times 5 \times 7$ m^3 volume featuring a VICON motion capture system comprising a total of 30 Vantage cameras. This high-performance system operates with sub-millimeter accuracy at 100 Hz.

A. Trajectory Tracking Test

The results of tracking a reference spherical Lissajous curve (26) are depicted in Fig. 6, and the video of the experiment can be found at `https://youtu.be/jZNbOG-ZYTc`. We conducted experimental comparison tests using the proposed controller and controllers designed in [29] and [16], all under identical conditions. The load mass information fed to the controller had a 40% discrepancy (0.03 kg instead of the actual 0.05 kg). In steady-state, the mean position errors are 3.01 cm and 7.36 cm for $v_d = 0.5$ m/s and $v_d = 1$ m/s, respectively. These values are smaller than the corresponding errors (3.07 cm and 10.24 cm; 8.61 cm and 12.00 cm) obtained by the controllers presented in [29] and [16]. The uncertainties in the system are visually revealed in the estimates. As expected, both estimates $\widehat{\boldsymbol{\Delta}}_{_{L/C}}$ are higher during the initial transient to compensate for partial nonlinear dynamics associated with the underactuation. Once accurate tracking is attained, they vary slightly, only to deal with external disturbances and unknown dynamics.

B. Disturbance Rejection Test

Our second test involved evaluating the disturbance rejection capabilities of the proposed controller.

1) Manually Induced Disturbances: to evaluate the controller's robustness to externally induced disturbances, we manually stroked the load four times while the QSLS was hovering. As shown in Fig. 7, each strike resulted in a sudden spike in the cable angular velocity ($\boldsymbol{\omega}$), with magnitudes reaching up to 100 deg/s. The plots in Fig. 7 demonstrate that the UDE-based controller's agile and prompt corrections effectively dampened the induced and undesired oscillations. Most importantly, rapid and effective responses from the UDEs are noticeable.

2) Constant Wind Disturbance: we conducted a hovering maneuver in the presence of constant disturbances generated by a mechanical fan (see results in Fig. 8). A video of the experiments can be found at `https://youtu.be/Gk7_q_0u6ek`. Following a period of 10 s with the system hovering in steady-state, we turned on a mechanical fan at $t = 10$ s, distanced one meter from the quadrotor, blowing a major wind flow pointing in the negative x direction, therefore generating a somewhat constant external disturbance. The fan was kept on for around 20 s. Afterwards, and while the system remained hovering, we turned off the fan and moved it to a different location, also distancing one meter from the quadrotor. Following a period of 10 s with the system hovering in steady-state, we turned on the fan. A major wind flow kept blowing for 20 s in the positive y direction. The results are plotted in Fig. 8. The three components of $\widehat{\boldsymbol{\Delta}}_{_L}$ quickly set in to counteract the wind action. Notice, in particular, that within the interval $t \in [10,\ 30]$ s, the x component settles around a negative

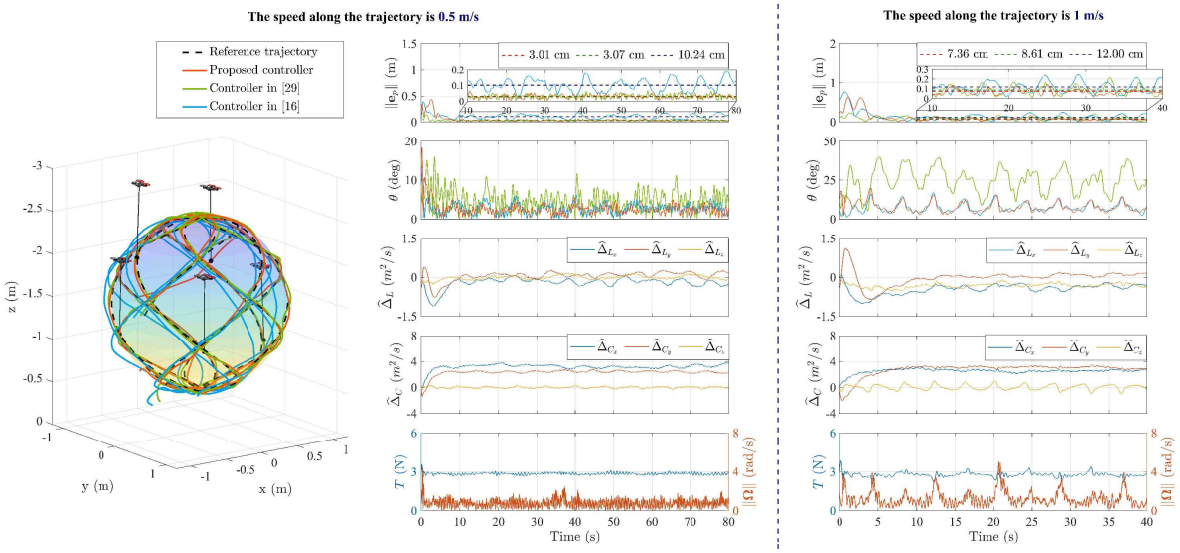

Fig. 6. On the left: the superposition of reference trajectory (26) and the actual trajectories. The QSLS is plotted at several time instants, with realistic representation of positions and attitudes. On the right (under two distinct reference speeds): the time evolution of position error magnitude, horizontal dashed lines depict mean values computed in steady state, with values showed in legends; the angle between the cable and the vertical defined as $\theta := \arccos(\mathbf{n}^{\mathsf{T}}\mathbf{e}_3)$; UDE estimates; and thrust and angular velocity control laws.

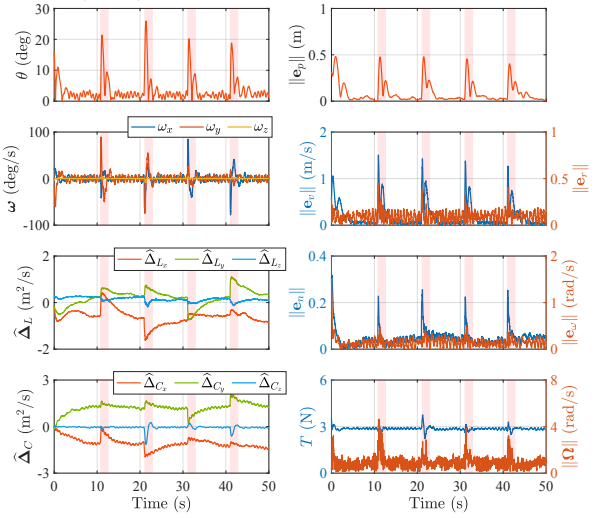

Fig. 7. On the left: angle θ between cable and vertical; load angular velocity $\boldsymbol{\omega}$; and UDE estimates $\widehat{\boldsymbol{\Delta}}_L$ and $\widehat{\boldsymbol{\Delta}}_C$. On the right: time evolution of tracking errors; and thrust and angular velocity control laws. Shaded bands are used to highlight periods of load disturbance and ensuing recovery.

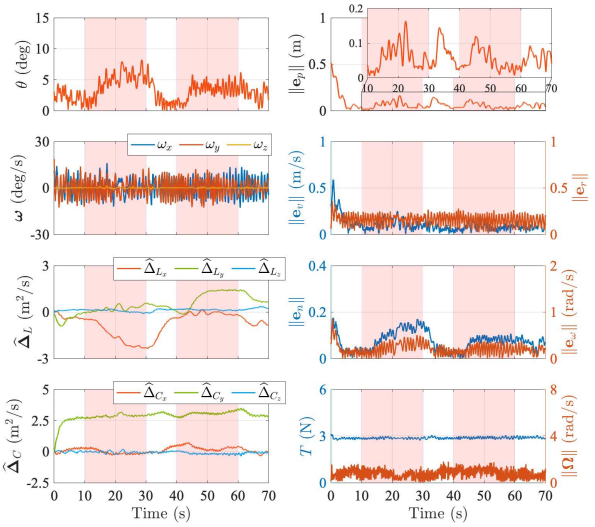

Fig. 8. On the left: angle θ between cable and vertical; load angular velocity $\boldsymbol{\omega}$; and UDE estimates $\widehat{\boldsymbol{\Delta}}_L$ and $\widehat{\boldsymbol{\Delta}}_C$. On the right: time evolution of tracking errors; and thrust and angular velocity control laws. Shaded bands are used to highlight periods of load disturbance and ensuing recovery.

value, which is consistent with the wind direction on the horizontal plane. Likewise, when the fan changes direction, the y component of $\widehat{\boldsymbol{\Delta}}_L$ change accordingly.

3) Disturbance Caused by the Offset of the Tethered Point: the results of load tracking the trajectory (26) in the presence of disturbances caused by an offset of the tethered point, were illustrated in case (c) of Fig. 1. The plots in Fig. 9 demonstrate that the proposed methodology exhibits robustness to the disturbances, as evidenced by a mean position error of only 3.6 cm and the convergence of estimates $\widehat{\boldsymbol{\Delta}}_L$ and $\widehat{\boldsymbol{\Delta}}_C$ throughout the entire maneuver.

4) Disturbance Caused by Uncertain Cable Length: the results of load tracking for the trajectory $\mathbf{p}_d(\gamma(t)) := [\sin(\gamma(t)), 2\sin(\gamma(t)/2), -2.15+\cos(\gamma(t))]^{\mathsf{T}}(\mathrm{m})$ in the presence of disturbances caused by uncertain cable length (a 20% discrepancy, 0.48 m instead of 0.6 m) are illustrated in Fig. 10. These plots demonstrate the robustness of the proposed methodology to parameter uncertainties, as evidenced by a mean position error of only 6.6 cm and the convergence of estimates $\widehat{\boldsymbol{\Delta}}_L$ and $\widehat{\boldsymbol{\Delta}}_C$ throughout the entire maneuver.

VIII. Conclusion

This study presented an UDE-based robust control approach for trajectory tracking of a QSLS. To simplify the control design, we employed a coordinate transformation strategy to convert the system into a standard quadrotor configuration. The proposed controller consists of nominal and robust components, with the nominal component handling trajectory tracking and the robust component compensating for lumped disturbances. We provided a thorough analysis of the robustness of the closed-loop control system. The designed control inputs ensure that the cable remains taut, and all error terms achieve uniformly ultimate boundedness.

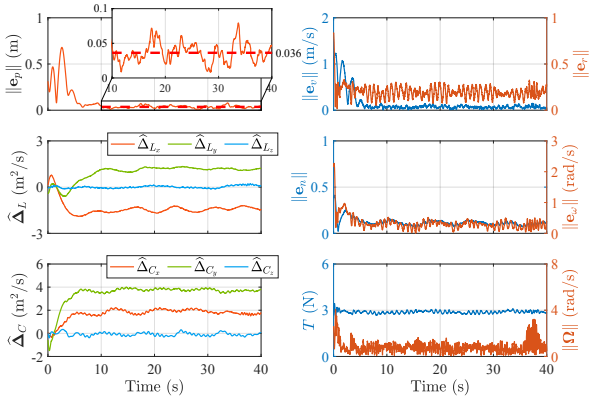

Fig. 9. Time evolution of the tracking errors; UDE estimates; and thrust and angular velocity control laws.

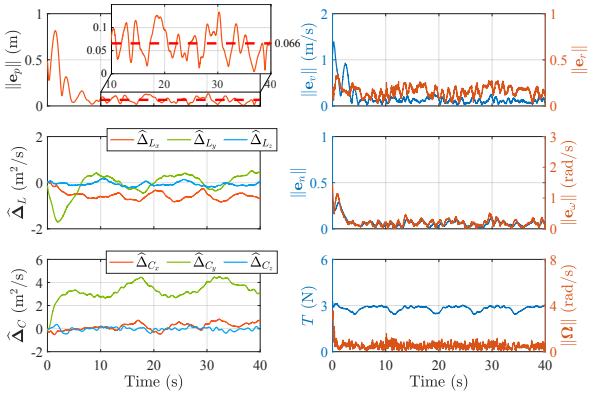

Fig. 10. Time evolution of the tracking errors; UDE estimates; and thrust and angular velocity control laws.

We presented both simulation and experimental results to demonstrate the effectiveness of the proposed control approach. A comparison with state-of-the-art works further confirms the good performance of our proposed solution.

REFERENCES

[1] A. Gawel, M. Kamel, T. Novkovic, J. Widauer, D. Schindler, B. P. von Altishofen, R. Siegwart, and J. Nieto, "Aerial picking and delivery of magnetic objects with MAVs," in *2017 IEEE International Conference on Robotics and Automation (ICRA)*, 2017, pp. 5746–5752.

[2] V. Ghadiok, J. Goldin, and W. Ren, "Autonomous indoor aerial gripping using a quadrotor," in *2011 IEEE/RSJ International Conference on Intelligent Robots and Systems*, 2011, pp. 4645–4651.

[3] C. C. Kessens, J. Thomas, J. P. Desai, and V. Kumar, "Versatile aerial grasping using self-sealing suction," in *2016 IEEE International Conference on Robotics and Automation (ICRA)*, 2016, pp. 3249–3254.

[4] B. E. Jackson, T. A. Howell, K. Shah, M. Schwager, and Z. Manchester, "Scalable cooperative transport of cable-suspended loads with UAVs using distributed trajectory optimization," *IEEE Robotics and Automation Letters*, vol. 5, no. 2, pp. 3368–3374, 2020.

[5] D. Sanalitro, H. J. Savino, M. Tognon, J. Cortés, and A. Franchi, "Full-pose manipulation control of a cable-suspended load with multiple UAVs under uncertainties," *IEEE Robotics and Automation Letters*, vol. 5, no. 2, pp. 2185–2191, 2020.

[6] S. Lee and H. Son, "Antisway control of a multirotor with cable-suspended payload," *IEEE Transactions on Control Systems Technology*, vol. 29, no. 6, pp. 2630–2638, 2021.

[7] J. Zeng, P. Kotaru, M. W. Mueller, and K. Sreenath, "Differential flatness based path planning with direct collocation on hybrid modes for a quadrotor with a cable-suspended payload," *IEEE Robotics and Automation Letters*, vol. 5, no. 2, pp. 3074–3081, 2020.

[8] C. Y. Son, H. Seo, D. Jang, and H. J. Kim, "Real-time optimal trajectory generation and control of a multi-rotor with a suspended load for obstacle avoidance," *IEEE Robotics and Automation Letters*, vol. 5, no. 2, pp. 1915–1922, 2020.

[9] X. Liang, Y. Fang, N. Sun, and H. Lin, "A novel energy-coupling-based hierarchical control approach for unmanned quadrotor transportation systems," *IEEE/ASME Transactions on Mechatronics*, vol. 24, no. 1, pp. 248–259, 2019.

[10] A. S. Brandão, D. Smrcka, É. Pairet, T. Nascimento, and M. Saska, "Side-pull maneuver: a novel control strategy for dragging a cable-tethered load of unknown weight using a UAV," *IEEE Robotics and Automation Letters*, vol. 7, no. 4, pp. 9159–9166, 2022.

[11] V. P. Tran, F. Santoso, M. A. Garrat, and S. G. Anavatti, "Neural network-based self-learning of an adaptive strictly negative imaginary tracking controller for a quadrotor transporting a cable-suspended payload with minimum swing," *IEEE Transactions on Industrial Electronics*, vol. 68, no. 10, pp. 10 258–10 268, 2020.

[12] G. Yu, J. Reis, D. Cabecinhas, R. Cunha, and C. Silvestre, "Reduced-complexity active disturbance rejection controller for quadrotor-slung-load transportation," *IEEE Transactions on Systems, Man, and Cybernetics: Systems*, 2023.

[13] G. Yu, J. Reis, and C. Silvestre, "Quadrotor neural network adaptive control: design and experimental validation," *IEEE Robotics and Automation Letters*, 2023.

[14] Z.-Y. Lv, Y. Wu, and W. Rui, "Nonlinear motion control for a quadrotor transporting a cable-suspended payload," *IEEE Transactions on Vehicular Technology*, vol. 69, no. 8, pp. 8192–8206, 2020.

[15] S. O. Ariyibi and O. Tekinalp, "Quaternion-based nonlinear attitude control of quadrotor formations carrying a slung load," *Aerospace Science and Technology*, vol. 105, p. 105995, 2020.

[16] Y. Wang, G. Yu, W. Xie, W. Zhang, and C. Silvestre, "Cooperative path following control of a team of quadrotor-slung-load systems under disturbances," *IEEE Transactions on Intelligent Vehicles*, 2023.

[17] I. Palunko, R. Fierro, and P. Cruz, "Trajectory generation for swing-free maneuvers of a quadrotor with suspended payload: A dynamic programming approach," in *2012 IEEE International Conference on Robotics and Automation*, 2012, pp. 2691–2697.

[18] K. Sreenath, T. Lee, and V. Kumar, "Geometric control and differential flatness of a quadrotor UAV with a cable-suspended load," in *52nd IEEE Conference on Decision and Control*, 2013, pp. 2269–2274.

[19] G. Yu, D. Cabecinhas, R. Cunha, and C. Silvestre, "Nonlinear backstepping control of a quadrotor-slung load system," *IEEE/ASME Transactions on Mechatronics*, vol. 24, no. 5, pp. 2304–2315, 2019.

[20] S. Tang and V. Kumar, "Mixed integer quadratic program trajectory generation for a quadrotor with a cable-suspended payload," in *2015 IEEE International Conference on Robotics and Automation (ICRA)*, 2015, pp. 2216–2222.

[21] D. Guo and K. K. Leang, "Image-based estimation, planning, and control of a cable-suspended payload for package delivery," *IEEE Robotics and Automation Letters*, vol. 5, no. 2, pp. 2698–2705, 2020.

[22] D. Hanover, P. Foehn, S. Sun, E. Kaufmann, and D. Scaramuzza, "Performance, precision, and payloads: adaptive nonlinear MPC for quadrotors," *IEEE Robotics and Automation Letters*, vol. 7, no. 2, pp. 690–697, 2021.

[23] N. Dalwadi, D. Deb, and S. Ozana, "Nonlinear disturbance observer-based backstepping control of tail-sitter quadrotors," in *Adaptive Hybrid Control of Quadrotor Drones*. Springer, 2023, pp. 19–42.

[24] ——, "Anti-swing control structure for the biplane quadrotor with slung load," in *Adaptive Hybrid Control of Quadrotor Drones*. Springer, 2023, pp. 131–151.

[25] J. Dai and B. Ren, "UDE-based robust boundary control for an unstable parabolic PDE with unknown input disturbance," *Automatica*, vol. 93, pp. 363–368, 2018.

[26] J. Trachte, F. Gonzalez, and A. McFadyen, "Nonlinear model predictive control for a multi-rotor with heavy slung load," in *2014 International Conference on Unmanned Aircraft Systems (ICUAS)*. IEEE, 2014, pp. 1105–1110.

[27] N. Dalwadi, D. Deb, and S. Muyeen, "Observer based rotor failure compensation for biplane quadrotor with slung load," *Ain Shams Engineering Journal*, vol. 13, no. 6, p. 101748, 2022.

[28] N. Dalwadi, D. Deb, and S. Ozana, "Partial rotor failure compensation for biplane quadrotor with slung load," in *Adaptive Hybrid Control of Quadrotor Drones*. Springer, 2023, pp. 109–129.

[29] L. Qian and H. H. Liu, "Path-following control of a quadrotor UAV with a cable-suspended payload under wind disturbances," *IEEE Transactions on Industrial Electronics*, vol. 67, no. 3, pp. 2021–2029, 2019.